nature communications

Article

https://doi.org/10.1038/s41467-024-55099-9

Bridged emulsion gels from polymer–nanoparticle enabling large-amount biomedical encapsulation and functionalization

Received: 8 May 2024

Accepted: 28 November 2024

Published online: 30 December 2024

Check for updates

Chuchu Wan[1], Si He[2], Quanyong Cheng[1], Kehan Du[1], Yuhang Song[1], Xiang Yu[1], Hao Jiang[1], Caili Huang[1] ✉, Jiangping Xu[1], Cong Ma[2] & Jintao Zhu[1]

Large-amount encapsulation and subsequent expressing are common characteristics for many biomedical applications, such as cosmetic creams and medical ointments. Emulsion gels can accomplish that, but often undergo exclusive, complex, multiple synthesis steps, showing extremely laborious and non-universal. The method here is simple via precisely interfacial engineering in homogenizing a nanoparticle aqueous dispersion and a polymer oil solution, gaining interfacial 45° three-phase-contact-angle for the nanoparticle that can bridge across oil emulsions' interfaces and ultimately form interconnected macroscopic networks. Their bridged skeletons and rheology are tunable over a vast range and deterministic on the basis of components' inputs. Furthermore, emulsion gels with high encapsulation and storage ability encapsulating active sunscreen ingredients, as a proof-of-concept, outperform commercial products. The ease (only seconds by strongly mixing two solutions) and the versatile chemical selection of our synthetic emulsion gels suggest an exciting general, scalable strategy for the next-generation cosmetic, ointment or otherwise food gel systems.

Emulsion gels with a structure of emulsion networks have both solid and liquid characters, such that they have been broadly applied in biomedical fields[1–3]. The former attributes allow them to be easily processed or shape-maintained, and the latter ones afford themselves the ability of large-amount encapsulation and on-demand delivery[4–6]. Simultaneously owning these two phases' features is unachievable to perform functions in certain biomedical cases by otherwise counterparts: solid, e.g. micelles or capsules[7–9]; liquid, e.g. emulsions[10]. For example, with regard to cosmetic creams and medical ointments, for absorption of antioxidants or antimicrobials, or maintenance of humidity, or realization of other functions, the ability to squeeze and subsequent finger or swab coating with suitable viscoelastic properties is desirable to enable hours stabilization, ingredient lock-in and adhesion. Another example is nursing-care foods, e.g. dysphagia foods: choking is prone to occur if pure liquids of nutriment or boluses were directly selected for dysphagic patients[11]; only emulsion gels, with tailorable rheology and tribology, can accomplish the high loading of nutrition ingredient and the comfortable and safe ingestion. Therefore, emulsion gels are emerging in a wealth of applications in cosmetics, skin cares, ointments, emulsion-based foods or drug- or ingredient-delivery[12–15].

Constructing emulsion gels can be done in diverse ways. The first method is gelation of the continuous phase of emulsions and locking-in the arbitrary movement of the dispersed droplets[16,17]. For the steps

[1]Key Laboratory of Materials Chemistry for Energy Conversion and Storage of Ministry of Education (HUST), School of Chemistry and Chemical Engineering, Huazhong University of Science and Technology (HUST), Wuhan 430074, China. [2]Key Laboratory of Molecular Biophysics of the Ministry of Education (HUST), College of Life Science and Technology, Huazhong University of Science and Technology (HUST), Wuhan 430074, China. ✉e-mail: cailihuang@hust.edu.cn

of gelation and emulsification, either one can proceed firstly and successively followed by the other one, or their hocket, i.e., emulsions are poured and dispersed into a pre-gelated bulk phase, or the fluids of continuous phase embracing emulsions are gelated by cross-linking or other weak interactions (e.g. Van der Waals force, hydrophobic effect or physical entanglement) of dissolved or dispersed components, or alternating of both[18]. These procedures usually involve high-temperature and long-time handling, along with intermittent mechanical blending, reminiscent of the lengthy decoction of traditional Chinese medicine ointment[19]. Connecting the dispersed emulsion droplets to form a three-dimensional network structure is another strategy for formulating gelled emulsions[20,21]. To this end, the droplet interfaces are usually bridged by mono- or double-layer particles that assemble at the water/oil interfaces. For a mono-layer case, particles are surface sophisticatedly designed to achieve a specific interfacial angle (three-phase contact angle) for a certain water/oil system that enables themselves as a monolayer structure to span two droplets' interfaces with an extremely thin continuous fluid between these two droplets, leading to an interconnected cluster and ultimately a macroscopic web, i.e., emulsion gels[21]. If, on the other hand, post-modification of particle-stabilized droplets is treated, e.g. interactions (cross-linking or supramolecular interaction) between particles are introduced, then droplets aggregate together, forming droplet networks with a double-layer particle bridged structure[22]. Although advances therein have been made in the manufacturing of emulsion gels[17,23–25], complicated, multiple steps and/or painstaking syntheses of the gel emulsifier–particles are inevitable, making their processes extremely laborious and non-universal. High necessity and urgency, therefore, lie here for designing a simple, versatile, and general method to prepare emulsion gels.

Here, we propose a simple strategy to fabricate bridged emulsion gels by employing a polymer to regulate the nanoparticle (NP) assembly at the water/oil interfaces. Before their cooperative assembly at the water/oil interfaces, the polymer (amine-terminated polydimethylsiloxanes, PDMS-NH_2) is dissolved in oil and the NP (negatively charged silica NP, SiO_2 NP) is dispersed in water and they have complementary interaction. With their dynamic character and self-regulation behavior, the number of polymer chains anchored to the NP at the interfaces can be easily tuned and, to approach ~45° of the NP's three-phase contact angle (with respect to the aqueous phase), by inputting at a range of their prescribed concentrations. These NPs with 45° bridge oil droplets with shared monolayer structure and form a connected droplet network. Although achieving such a specific three-phase contact angle of the NPs is extremely stringent for otherwise counterparts, the NPs, herein, tailored by the polymers, can be realized by a wide range of conditions, including spanning orders of magnitude for the concentration range of both components and the water/oil mixing ratio (8/2 – 3/7). As such, by varying the parameters that govern the interface skeleton, the rheological properties of the obtained emulsion gels can be tuned, e.g. storage modulus, over three orders of magnitude. Based on such emulsion gels with tunable formulation and viscoelasticity, an effective sunscreen for skin ultraviolet (UV) protection, as a model of biomedical application, is developed and, showcases superior to the performance of L'Oreal sunscreen. The other merit is that our synthetic sunscreens take only seconds by mixing those water and oil phases. The ease with which the emulsion gel systems can be manufactured—with the versatility that the NP, the polymer, and the oil phase can all be varied—guides new directions in designing the next-generation emulsion gel materials for large-amount encapsulation and delivery cargos in food and biomedical industries, that far beyond what we demonstrated here. Specifically, all these components consist of biomaterials (e.g. NPs are protein- or polysaccharide-based) and, could be suited for foods for individuals who struggle with mastication and deglutition.

Results

The nanoparticles (NPs), selected herein, were commercial silicon dioxide (SiO_2) NPs (diameter ~12 nm) with negatively charged surfaces (Si-O^- groups[26], Supplementary Figs. 1 and 2) and dispersed in water. They were not interfacially active when their aqueous solution (0.5% *w*/*w*) contacted the oil phase, e.g. toluene, owing to the inherent negative charge of the water/toluene interfaces[27], as evidenced by the very close of the interfacial tension ($\gamma \approx 34.5$ mN m^{-1}) to that value between pure water and toluene (~36 mN m^{-1}) (Fig. 1a). Moving to the water/toluene interfaces of the NPs was driven by the introduction of amine-terminated polydimethylsiloxanes (PDMS-NH_2, molecular weight, MW = 1000 g mol^{-1}) into the toluene phase (0.05% *w*/*w*), where the polymer chains of PDMS-NH_2 assembled to the water/toluene interfaces firstly as a monolayer[27] and gradually reduced γ to 26 mNm^{-1} at 750 s, transforming into PDMS-NH_3^+ due to the pH of aqueous dispersion ~7.0 and the pK_a of $-NH_2$ ~9[28], and they then recruited the NPs together at the interfaces via electrostatic interaction, forming a polymer–NP monolayer[29,30]. The assembly of the SiO_2 NPs assisted by the PDMS-NH_2 is quite different from the polymer itself. This can be found in the interfacial energy reduction, where there was a quick initial decrease followed by a slow reduction in γ to a quasi-state equilibrium ($\gamma_{qu\text{-}eq} \approx 13$ mN m^{-1}). The former obviously originated from the recruitment of the NPs by the polymers that covered the interfaces quickly, and the latter included the rearrangement of polymer–NP ensembles and re-recruitment by vacated space[31], showing the self-regulation behavior of cooperative polymer–NP ensembles or controllable manner of the NPs at the interfaces by the polymers.

Based on this exclusive controllable behavior of the NPs, if we use relatively low amount of the polymers to the number of the NPs, achieved by tailoring concentration ratio, the NPs would be attracted by sparse polymers at the interfaces upon homogenizing the mixtures of the NP aqueous solution (4% *w*/*w*) and the toluene solution of PDMS-NH_2 (3% *w*/*w*) with a mixing ratio of 5:5 (*v*/*v*), i.e., strong emulsified. The NPs anchoring a few hairs of the polymers would have a low three-phase contact angle with respect to the aqueous phase, such that the NPs have a strong tendency to cross over and occupy two oil droplets' interfaces (here o/w emulsions are definitely formed) and tweezer very thin water phase, rather than stabilizing single droplets (Fig. 1b, c). Note that: although the polymer concentration is not so low, the effective number of the polymer chains at the water/toluene interfaces that attract the NPs together does be few. In other words, the initial assembly of the polymers at the interfaces is sparse and, then they attracted the NPs from water immediately other than only waiting for more polymers' arrival from the toluene bulk phase. This can be found in the evidence from the interfacial tension reduction data, where the cooperative assembly occurs quickly in the first 10 s while the reduction in γ for the polymer alone is very slow and continuous for hundreds of seconds. Reversely inferring from the emulsion results, it is also impossible that all polymers assembly first to the interfaces, spending at least hundreds of seconds, and in turn attract the NPs, since the cooperative ensembles have strong interfacial activity such that they can stabilize smaller emulsions generated by the strong homogenization (polymers alone cannot stabilize emulsions, Supplementary Fig. 3). As a result, spanning the interfaces of two droplets by the NPs, along with the evolution of the small, emulsified droplets (capillary bridge formation and coalescence), lead to the jamming of bridged emulsions, i.e., forming the bridged emulsion gels that show long-term stability over 12 months. Detailed discussion on the concentration range of the NPs and the polymers will be held in the following (*vide infra*).

To visualize the monolayer and precise structure of the NPs between the closely neighbored droplets, we used another larger SiO_2 NPs (diameter ~630 nm) fluorescence labeled by rhodamine B isothiocyanate (RITC) (Supplementary Fig. 4), that also have negatively

https://doi.org/10.1038/s41467-024-55099-9

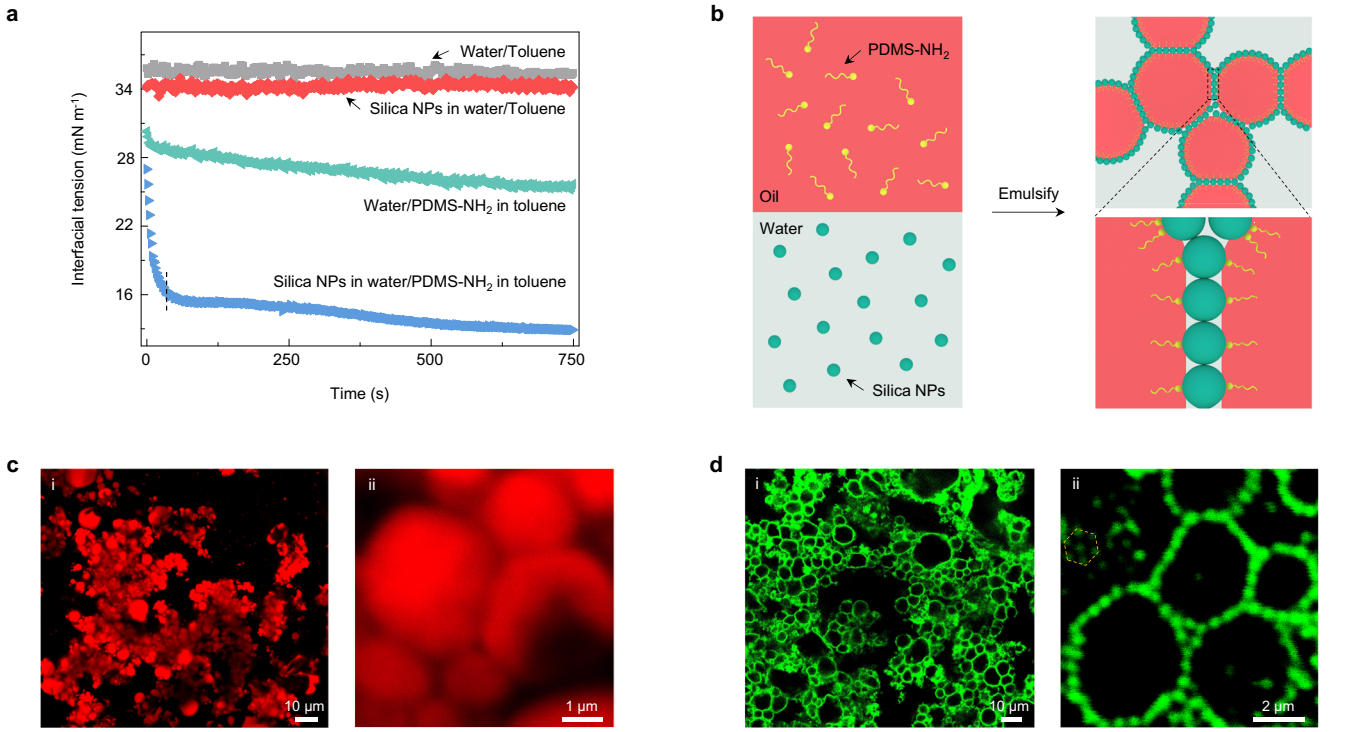

Fig. 1 | Formation and structure of bridged emulsion gels. a The recruitment of negatively charged SiO_2 NPs to the interfaces by PDMS-NH_2 occurs on different time scales and depends on the relative concentration of each. These processes can be observed by monitoring the interfacial tension as a function of time for a pendant water drop suspended in a bath of toluene for systems configured with either nothing (gray squares), SiO_2 NPs (red rhombuses), PDMS-NH_2 (green triangles), or SiO_2 NPs + PDMS-NH_2 (blue triangles). The concentration of SiO_2 NPs in water is 0.5% *w*/*w* and the concentration of PDMS-NH_2 in toluene is 0.05% *w*/*w*. **b** Schematic showing the formation of bridged emulsion gels by employing the polymers to regulate the NP assembly at the water/oil interfaces. The polymers (PDMS-NH_2), and the NPs (negatively charged SiO_2 NPs), are dissolved in oil and dispersed in water, respectively. When emulsifying the oil and water phase, a few polymer chains attach to the NPs at the interfaces, gaining the three-phase contact angle of ~45° (with respect to the aqueous phase) of the NPs. These NPs with 45° bridge across droplets' interfaces and ultimately form an interconnected macroscopic network. **c** Low-magnification (i) and high-magnification (ii) confocal microscopy images of bridged emulsion gels showing adhesive oil droplets in the continuous aqueous phase as the oil phase is stained with Nile red. [SiO_2 NPs] = 4% *w*/*w*, [PDMS-NH_2] = 3% *w*/*w*, water/oil ratio is 5:5 (*v*/*v*). **d** Low-magnification (i) and high-magnification (ii) confocal microscopy images of bridged emulsion gels showing a monolayer of particles bridging numbers of faceted droplets as the particles are tagged with rhodamine B isothiocyanate (RITC). [SiO_2 NPs] = 8% *w*/*w*, [PDMS-NH_2] = 3% *w*/*w*, water/oil ratio is 5:5 (*v*/*v*). The yellow hexagonal dotted box showing approximate hexagonal packing of the NPs.

charged surface (similar zeta potential value, without interfacial activity) and can co-assemble with PDMS-NH_2 (Supplementary Figs. 5 and 6). It was found that numbers of polygonal droplets abounded with the whole system, very similar to the case based on the smaller NPs in Fig. 1c but having a clearer visualization of the interfaces (Fig. 1d and Supplementary Fig. 7). Zooming in the interfaces between droplets [Fig. 1d(ii)], a monolayer structure of the NPs with approximate hexagonal packing, constructing the skeleton that interconnected droplets and the formed network, was obviously seen. Such locally ordered monolayer packing of the NPs at the interfaces testifies to the rearrangement of polymer–NP ensembles. The further details of the NPs at the interfaces were characterized by solidifying water and oil, i.e., using cryo-scanning electron microscopy (cryo-SEM) method[32] (Supplementary Fig. 8). It was found that the NPs had a three-phase contact angle of ~45° at the interfaces, just at the middle point between neutron wetting (90°) and non-interfacial activity (0°), showing strong evidence for the NPs bridging over droplets.

Insight into the formation mechanism and structure of these bridged emulsion gels is given by studying the parameters that govern their stability, morphology, and domain size. Given that the SiO_2 NPs are attracted by the PDMS-NH_2 chains to the interfaces, the number of the NPs in water naturally affects their being recruitment kinetics, and eventually the interface skeleton. Here, we still used the small NPs since they can provide more effective interface coverage (*vide supra*). If we decreased or increased the concentration of the NPs (C_N, from 2% to 8% *w*/*w*) on the basis of the sample in Fig. 1c, it was found that all samples in these C_N ranges were bridged emulsion gels, and their average droplet diameter (D) decreased from 8.3 ± 2.2 to 2.1 ± 0.8 and 1.5 ± 0.5 μm with increasing C_N (Figs. 1c and 2a, Supplementary Figs. 9 and 10). Such a decrease was derived from the fact that the higher concentration of the NPs can cover more interfaces. Varying C_N did not change the bridged droplets' structure, meaning that the three-phase contact angle was almost kept at ~45°. This can be attributed to the simultaneous multiple evolved processes in the formation of bridged droplets, including the attraction of the NPs, the rearrangement of polymer–NP ensembles, and the evolution of droplets (i.e., coalescence of droplets), leading to that the increased numbers of the NPs were recruited by the other polymer chains at the interfaces and thus occupied more interfaces (i.e., smaller droplets). And, along with the droplets' Ostwald Ripening, the tendency of NPs crossing over oil droplets does not change such that the anchoring number of polymers to one NP keeps consistent in forming monolayer bridged structure. Further extreme concentration of the NPs gave rise to the derivation of this three-phase contact angle, as for example at the lower value of C_N (<1% *w*/*w*) the system formed dispersed emulsions (*vide infra*). This mechanism is also supported by the failure formation of emulsion gels by vortex mixing (Supplementary Fig. 11), due to the inability to bridge large droplets at their slow Ostwald Ripening but fast co-assembly of polymer–NP. If, on the other hand, the C_N was fixed at 4% *w*/*w*, we varied the functional polymer concentration (C_P), from 1% to 10% *w*/*w*. It was found that the two samples based on preparation from 1% [Fig. 2b(i)] and 3% (Fig. 1c) *w*/*w* C_P had similar features on domain size

https://doi.org/10.1038/s41467-024-55099-9

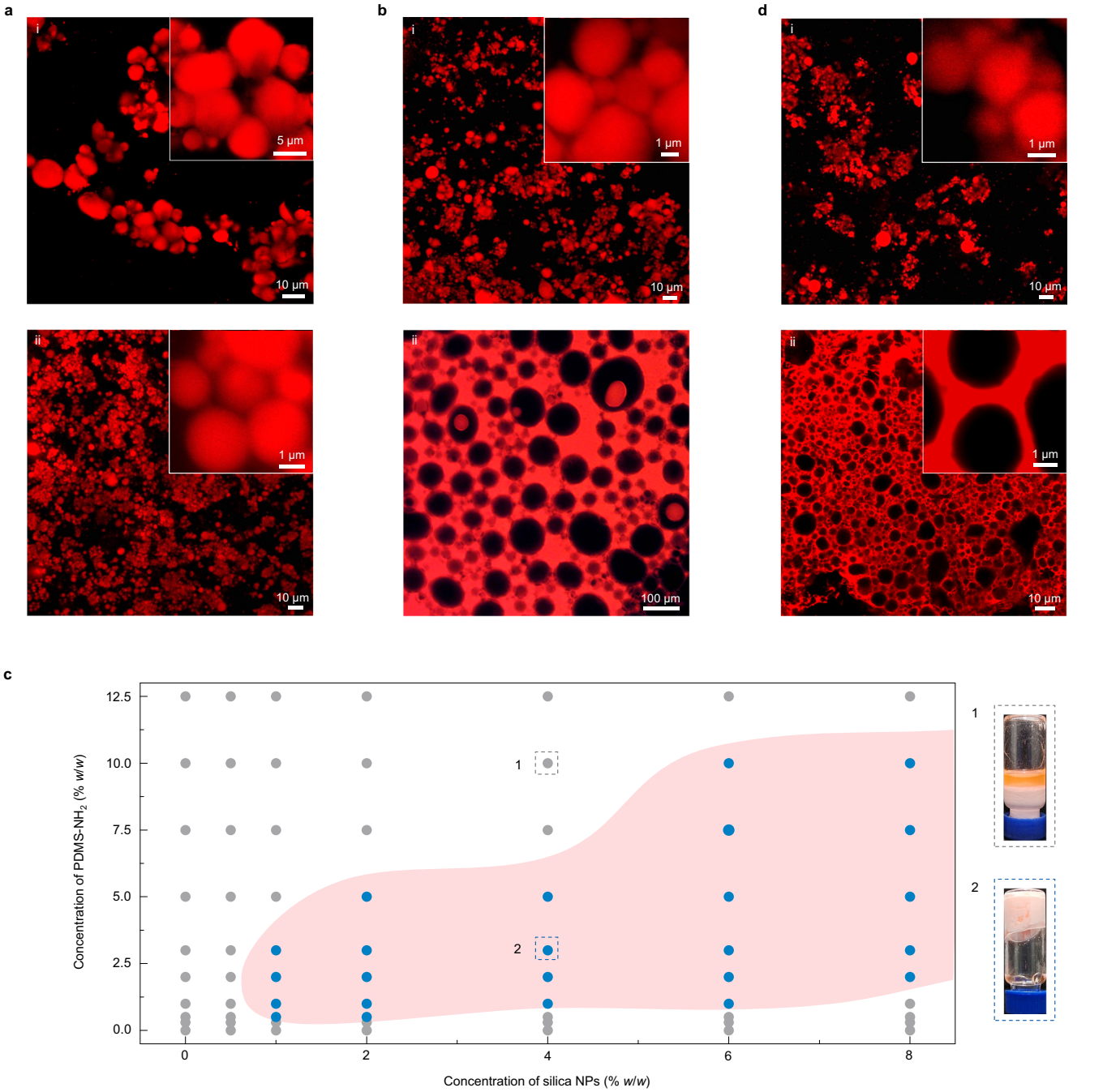

Fig. 2 | Impact of altering the particle and polymer concentration, and the water/oil volume ratio upon system morphology. a Bridged emulsion gel systems formed by polymer–NP ensembles with a NP concentration of (i) 2% *w*/*w* and (ii) 8% *w*/*w* at a fixed concentration of PDMS-NH_2 (3% *w*/*w*). Water/oil ratio is 5:5 (*v*/*v*). **b** Emulsion systems formed by polymer–NP ensembles at constant NP concentration (4% *w*/*w*) with varying concentrations of PDMS-NH_2 from (i) 1% *w*/*w* to (ii) 10% *w*/*w*. Water/oil ratio is 5:5 (*v*/*v*). **c** Phase diagram of bridged emulsion gels prepared by different concentrations of NPs in water and PDMS-NH_2 in toluene. Water/oil ratio is 5:5 (*v*/*v*). The gray and blue circles correspond to emulsions and bridged emulsion gels, respectively; typical appearances are shown as 1 and 2. The red area highlights the experimental conditions leading to bridged emulsion gels. **d** Emulsion gel systems formed by polymer–NP ensembles with the volume ratio of the water to the oil phase of (i) 8:2 and (ii) 2:8. [SiO_2 NPs] = 4% *w*/*w*, [PDMS-NH_2] = 3% *w*/*w*.

(D: 2.3 ± 0.5 and 2.1 ± 0.8 μm), indicating that in these C_P ranges, there is imperceptible difference between their polymers' assembly kinetics (Supplementary Fig. 12), particularly in the initial stage, dictating their attraction of the NPs and then the construction of the interfaces. This is consistent with our mentioned proposal above that numbers of polymer chains stay in the oil bulk phase. This result is also evidence that the contact angle of the NPs keeps at ~45° in a certain range of C_P, as more directly testified by NP monolayer bridged emulsion gels formed using large NP (630 nm) with a certain range of PDMS-NH_2 concentration (Supplementary Fig. 13). Such a rule will be invalid upon C_P over 5% *w*/*w* (Fig. 2c). For example, when C_P was increased to 10% *w*/*w* [Fig. 2b(ii)], much larger water-in-oil (w/o) emulsion droplets (91.1 ± 21.9 μm) were observed due to an excess of PDMS-NH_2 chains anchoring to the NPs, inducing polymer–NP ensembles to transform from hydrophilic to hydrophobic and finally inversing the curvature of the interfaces[33]. The excessive polymer chains alone having different assembly behavior was also testified by the much lower, plane interfacial tension without the successive decrease (Supplementary Fig. 12).

In the opposite direction, too few polymer chains (C_P < 1% *w*/*w*) led to a typical o/w emulsion or even a non-stable emulsion (Fig. 2c). As such, it was summarized for the phase diagram of the concentrations of the NP and the polymer about the zone of bridged emulsion gels (Fig. 2c). We note that our samples have over 97% gel structures, where typical one is shown in the lower right corner of Fig. 2c. We find that the necessary conditions for the formation of these bridged emulsion gels include a sufficient concentration of NPs and an appropriate concentration range of polymers.

Varying the mixing ratio of the NP aqueous solution to the oil solution of the polymer when fixing the two components' concentration is another alternative to tailor the morphology of the bridged emulsion gel system. Here, we prepared a series of samples with variations of volume mixing ratio between 8:2 and 2:8, using 4% *w*/*w* NP aqueous solution and toluene solution of 3% *w*/*w* PDMS-NH_2. It was found that the samples prepared from mixing ratios of 8:2–3:7 were NP monolayer structured bridged emulsions with *D* monotonically increasing from 1.3 ± 0.4 to 5.9 ± 1.6 μm (Fig. 2d and Supplementary Fig. 14). This increase is an indication that the NPs play a key role in determining the emulsion droplet size, since their equivalent C_N values are decreased from 6.4% to 2.4% *w*/*w*, with the variation of C_P between 1.2% *w*/*w* and 4.2% *w*/*w* (Supplementary Table 1), if they are considered by mixing with 5:5. Their equivalent concentrations in Fig. 2c constitute a line with a minus slope that passes the point of sample 2, and locate in gel zone. However, the sample with the mixing ratio at 2:8 showed a completely different morphology, a w/o emulsion gel structure. We note here two points: the first is that it is totally different from the sample in Fig. 2b(ii); its equivalent concentrations in Fig. 2c are 1.6% *w*/*w* (C_N) and 4.8% *w*/*w* (C_P), both lower than the half of the sample's concentrations in Fig. 2b(ii), but it has a much smaller polygonal emulsion droplet size (4.7 ± 2.0 μm); the second is that it does be a gel, showing a non-flowing character (similar to the inverted vial of sample 2 showed in Fig. 2c). This gel structure is not NP mono- or double-layer bridged morphology since the oil gap is larger as 200–500 nm [insert of Fig. 2d(ii)]. Its mechanism may arise from the synergy of two driving forces: its equivalent concentrations in Fig. 2c lie in the edge of the gel zone, giving the ability to form bridged emulsion gel, where a NP monolayer bridged gel would be obtained if the same concentrations are selected with 5:5 mixing; the high volume content of oil phase imparts a strong tendency to phase inversion to w/o type[34]. As such, these two loading forces, somehow, stabilize this gel structure. The bridged structures of those emulsion gels are further confirmed by Gaussian curvature distribution analysis (Supplementary Fig. 15). All curves show a sharp peak at $K = 0$ and their asymmetry at the right shoulder (the droplet networks' boundaries generate the positive Gaussian curvature), suggesting that most of the droplets are planar in the boundary shared bridged strucutres[21]. Additionally, we successfully form bridged emulsion gels systems using other functional polymers, as for example amine-terminated polystyrene (PS-NH_2), or changing the oil phase, such as *n*-hexane or tricaprylin (Supplementary Fig. 16), showing their universality.

Having quantified the parameter range to manufacture emulsion gels, we then probed their rheological properties and the correlation with the interface skeleton, dictating their processing and relevant applications. Here, we conducted oscillatory rheology to investigate their stress–strain response to the shear deformation. Another batch of samples was prepared with the variations of C_N from 1%–12% *w*/*w* at a fixed C_P of 3% *w*/*w* and mixing ratio of 5:5 *v*/*v*. Frequency sweep testing results showed that all samples had around one order of magnitude of storage modulus (*G′*) higher than the loss modulus (*G″*) and exhibited almost frequency-independent behavior, which are hallmarks of all samples' elastic character that are contributed by the percolating networks of bridged droplets[35] (Fig. 3a). Between these samples, *G′* and *G″* increased with higher NP loading due to the increased interfacial networks constructed by the NPs (*vide supra*), as for example *G′* increased from 912 to 11,200 Pa, an order of magnitude enhancement, when the NP loading increased from 1% to 12% *w*/*w*. For the strain sweep measurements (Fig. 3b), the values of *G′* and *G″* at the lower strain region (≤ 0.25%), a nearly planar linear viscoelastic region, showed a similar tendency with the data in frequency sweeping. As the strain increased, *G′* and *G″* decreased, and the former had a faster reduction, such that there were cross intersections between them, where the stress was called yield stress (τ_y). After that, *G″* was dominated over *G′*, where the gel networks were destroyed, exhibiting a fluid character. Figure 3c showed the apparent viscosity of these four samples as a function of frequency, and a typical shear-thinning behavior for all samples was observed, showing non-Newtonian fluids rather than dispersed emulsions[36].

In consideration of the assembling of the NPs regulated by the polymers, we then probed the impact of altering the concentration of PDMS-NH_2 upon system rheology. When we fixed C_N at 4% *w*/*w*, the values of *G′* and *G″* at the very low region (0.1% <strain <0.25%), or called G'_0 and G''_0, were found to increase from 1,335 to 3,260 and to 3,750 Pa, and from 55 to 155 and to 167 Pa, respectively, as C_P increased from 1% to 3% and to 5% *w*/*w* (Fig. 3d and Supplementary Fig. 17). There was a subtle increase for the last two samples, demonstrating that storage and loss modulus are dominated by the NPs and are auxiliary under the functional polymers. These results come to the conclusion that the stress–strain response of the bridged emulsions is derived from the mechanical transmission of shared facets between these polygonal droplets, that is contributed by the penetrating networks of the monolayer NPs assisted by the polymers on the microscale. As such, the NPs make a main contribution to the resistance to the deformation, and the PDMS-NH_2 chains play an irreplaceable role in biting the NPs together through their entanglement of the casual chains at the interfaces and the chains anchored to the NPs, since there is no attraction interaction, but repulsion, between the NPs (*vide supra*). Therefore, we plotted the G'_0 and τ_y as a function of C_N (Fig. 3e). One can see that both G'_0 and τ_y showed power–law relationship with C_N, as $G'_0 \sim C_N^{1.25}$, and $\tau_y \sim C_N^{1.56}$. Such scaling law is different from the emulsion gels bridged by the sole NPs[21], that have $G'_0 \sim C_N^{3.00}$ and $\tau_y \sim C_N^{1.90}$. This difference points to that using the functional polymers to manipulate the monolayer structure of the NPs not only circumvents the sophisticated syntheses of the NPs, but also weakens the exponent relation between G'_0 and C_N. Double-layer NPs bridged or other NPs prepared emulsion gels have a much stronger exponent contribution of C_N to G'_0 ($G'_0 \sim C_N^{>3.70}$)[21], further demonstrating the uniqueness of our system. Polymer chains manipulating the NPs and entangling between participants of vacant at the interfaces and anchoring to the NPs, that imparts the whole penetrating networks stronger viscoelasticity, can be found more evidence from that our system has a higher G'_0 than the sole NPs bridged case, as for example at 8% *w*/*w* C_N, G'_0 equals to 9,310 and 5,954 Pa[21], respectively.

Our system is also totally different from the case that owns a high volume fraction of dispersed droplets (high internal phase emulsions, HIPEs) that are prepared from surfactants or particles[37,38]. The emulsion system of high volume dispersed phase although has closed-packed droplets, its deformation response has a different characteristic since the continuous phase interspace between droplets makes the mechanical transmission and stress deformation occur randomly, instead of in an ordered, penetrating manner (our system). As a result, it has at least an order of magnitude lower value of G'_0 compared to our emulsion gels at approximately equal loading of particles or surfactants[39]. Further, to keep the HIPE system elasticity, the volume fraction of the dispersed phase must be >74%. In stark contrast, our emulsion gels can vary the water phase from 80% to 20% *v*/*v*, i.e., the mixing ratio of the aqueous solution to the oil phase from 8:2 to 2:8. Here, we probed the dependence of these mixing ratios on the system rheology. As shown in Fig. 3f and Supplementary Fig. 18, the sample with 5:5 mixing from the aqueous solution and the oil phase had the

https://doi.org/10.1038/s41467-024-55099-9

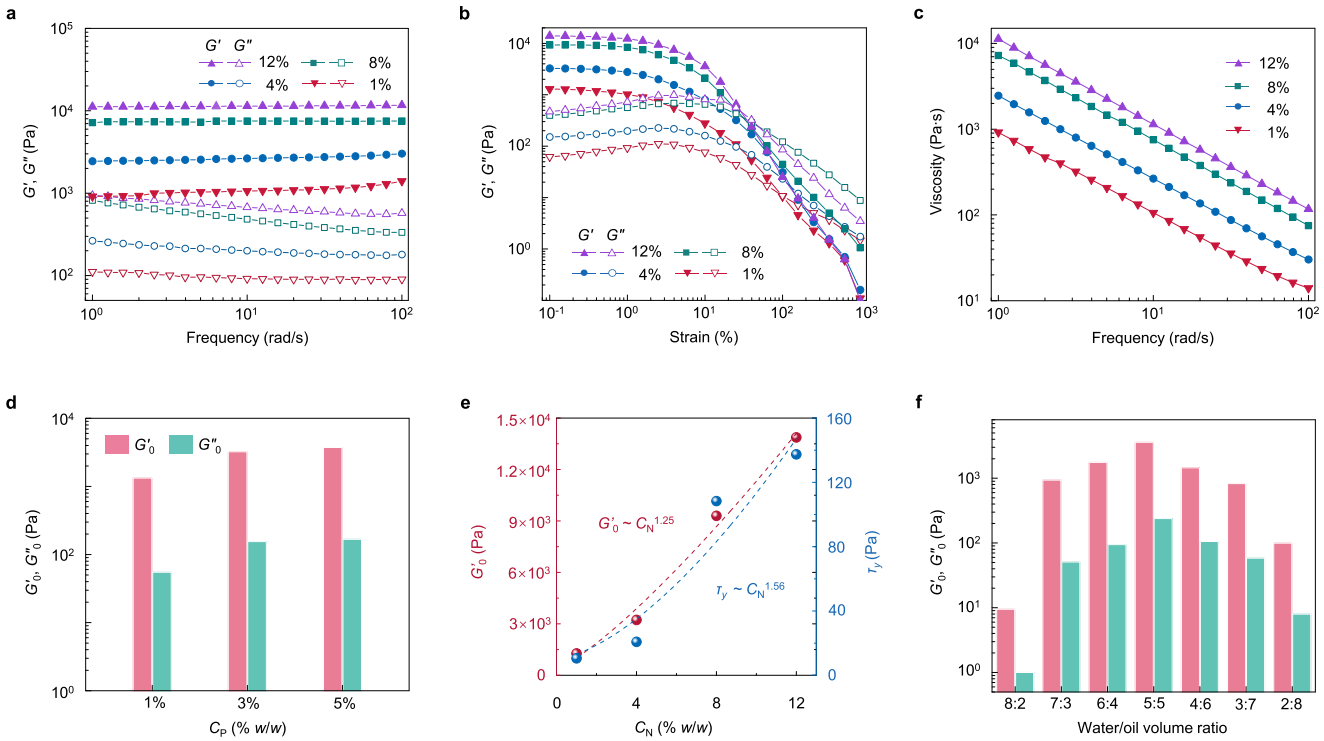

Fig. 3 | Viscoelastic properties of bridged emulsion gels and their tunability. **a** Frequency sweeps of storage modulus G' and loss modulus G'' of bridged emulsion gels with different C_N. [C_P] = 3% *w*/*w*, water/oil ratio is 5:5 (*v*/*v*). The strain is kept constant at 1%. **b** Strain sweeps of G' and G'' of bridged emulsion gels with different C_N. [C_P] = 3% *w*/*w*, water/oil ratio is 5:5 (*v*/*v*). The frequency is kept constant at 10 rad s^{-1}. **c** Frequency sweeps of viscosity of bridged emulsion gels with different C_N. [C_P] = 3% *w*/*w*, water/oil ratio is 5:5 (*v*/*v*). The strain is kept constant at 1%. **d** Zero-shear storage modulus G'_0 and zero-shear loss modulus G''_0 of bridged emulsion gels with different C_P. [C_N] = 4% *w*/*w*, water/oil ratio is 5:5 (*v*/*v*). **e** Scaling of G'_0 and yield stress, τ_y, of bridged emulsion gels with C_N. [C_P] = 3% *w*/*w*, water/oil ratio is 5:5 (*v*/*v*). **f** G'_0 and G''_0 of bridged emulsion gels with different volume ratios of the water to the oil phase varying from 8:2 to 2:8. [C_N] = 4% *w*/*w*, [C_P] = 3% *w*/*w*.

highest values of G'_0 and G''_0 (3,580 and 238 Pa), while the sample from 8:2 mixing had the lowest G'_0 and G''_0 (10 and 1 Pa). Although the 8:2 sample had the highest number of NPs, the 5:5 sample had a larger volume of oil phase that constructs the bridged networks, contributing to the rheological properties. In the opposition, the 4:6 and 3:7 samples had larger fractions of the oil phase, yet larger droplets with lower loading of the NPs, showing relatively weaker resistance to deformation in comparison to the denser, smaller droplets of the 5:5 sample. Specifically, the 2:8 gel sample with a w/o type structure showed lower G'_0 and G''_0 than the 3:7 bridged o/w emulsion gels. This dependence of rheology on the mixing ratio further demonstrates that the viscoelasticity of our system stems from polygonal droplets with shared facets on the macroscale that are constructed by the monolayer NPs regulated by the polymers on the microscale. In addition, all the emulsion gels show high stability over a wide range of pH (5–10) and ionic strength (NaCl, 0–200 mM) and against centrifugation (861 × g), high-temperature resistance (60 °C), and freeze-thaw stability (−23 °C) (Supplementary Figs. 19–23), reflecting an excellent encapsulation and storage ability.

These tunable (over orders of magnitude) viscoelastic emulsion gels, are well-suited for encapsulation and on-demand delivery of bioactive compounds in different biomedical applications. Here, β-carotene, a highly polyunsaturated nutraceutical that is extremely susceptible to oxidative degradation and loses its biological functions[40], was selected as a model molecule to be encapsulated in our emulsion gels. To achieve a large-amount encapsulation, we chose an emulsion gel system with a water/oil mixing ratio at 3:7, that also has high storage modulus, and the detail formulations are: an *n*-dodecane solution (560 μL) of β-carotene (0.1% *w*/*w*) and PDMS-NH_2 (3% *w*/*w*) was homogenized with aqueous dispersions (240 μL) of SiO_2 NPs, where the concentration of NPs was varied from 1% to 2% and 4% *w*/*w* to see its impact on encapsulation efficiency. A control sample was prepared, where it was bulk *n*-dodecane and contained the same content of β-carotene. All samples were flushed with a nitrogen stream for 15 min to exclude the oxygen and placed in a 37 °C water bath for a periodic detection of the retention of β-carotene as long as 35 days. The retention of β-carotene was analyzed by ultraviolet–visible (UV–vis) spectroscopy of the oil phase that was collected from the extractions using a certain amount of hexane three times after demulsifying by the introduction of ethanol and the treatment of vortex mixing (details see Methods). As shown in Fig. 4a and Supplementary Table 2, for the control sample, the retention of β-carotene decreased significantly over time and was only 13.5% at the end of testing, suggesting a continuous, strong oxidative degradation of β-carotene induced by the oxygen radicals generated at the oil/air interfaces (from the residual oxygen above the sample in the sealed vial) and their diffusion in the oil phase (our experiments were conducted under dark condition). In stark contrast, β-carotene encapsulated in bridged emulsion gels exhibited enhanced stability with the retention >87% after 35 days of testing. This can be attributed to the jamming interfacial layer of polymer–NP ensembles that provide a sufficient barrier to retard the diffusion of pro-oxidants or free radicals from the continuous water phase to the dispersed oil droplets. Between the emulsion gels, raising C_N led to an increase in the retention of β-carotene encapsulated in emulsion gels, e.g. increasing C_N from 1% to 4% *w*/*w* results in the retention increase from 87.5% to 96.4% on 35th day, pointing to a strong encapsulation and storage ability of emulsion gels with high NPs loading. Such a subtle loss of β-carotene stems from denser, smaller droplets-based gel networks, i.e., stronger armors on the oil droplets, that formed by higher particle concentrations (*vide supra*). Based on this, encapsulated β-carotene in bridged emulsion gels had superior resistance to ultraviolet (UV) (with a retention of

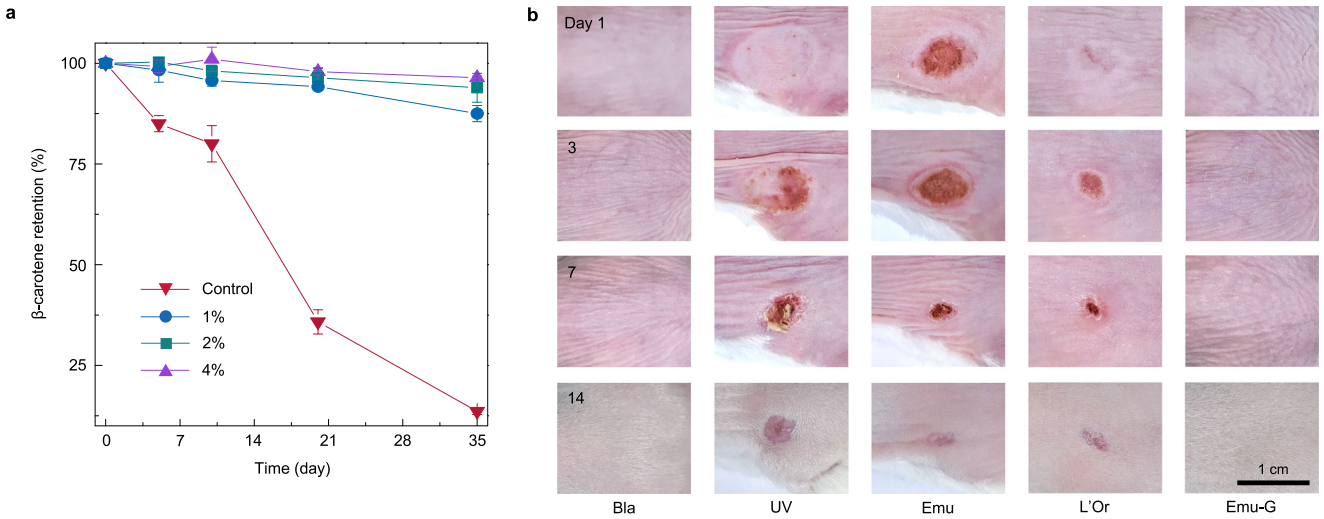

Fig. 4 | Effective encapsulation of bioactive ingredients of emulsion gels, and their in vivo protection against UV-induced skin burn. a The storage stability of β-carotene loaded in the dispersed oil phase of bridged emulsion gels in a 37 °C water bath after storage for 35 days as a function of C_N. [C_P] = 3% *w*/*w*, water/oil ratio is 3:7 (*v*/*v*). Bulk oil loaded with the same content of β-carotene in a 37 °C water bath served as the control. The retention of β-carotene was analyzed by using UV–vis spectroscopy to determine the β-carotene content in the oil phase at different time intervals. Data are presented as mean values ± SD (n = 3). **b** Representative images of mouse dorsal swabbed with different protective samples followed by UV irradiation on 1st day through 14th showing their sun protection effect. Bla represents the blank group, that mice were neither coated with samples nor irradiated with UV spot. UV represents the UV group, that mice were treated with UV irradiation. Emu, L'Or, and Emu-G represent the emulsion, L'Oreal and emulsion gel groups, that mice were swabbed with the same amount of emulsion, L'Oreal sunscreen, and emulsion gel sample before UV irradiation, respectively.

93.7% after 6 h of UV exposure) and thermal stability (with a retention of 95.8% at 70 °C) (Supplementary Figs. 24 and 25). Given the tunability of our system, water-soluble bioactive compounds, if desired, can be encapsulated in the w/o emulsion gel with a water/oil mixing ratio at 2:8 (*vide supra*).

Based on the robust encapsulation and storage ability of these emulsion gels, we applied our gels to skin protection, exploiting sunscreen cream as a prototypical model. Here, mimicking the commercial sunscreen cream, anti-sunburn ingredients, including three types of chemical sunscreen active compounds (methylene bis-benzotriazolyl tetramethylbutyl phenol, 8% *w*/*w*, ethylhexyl triazone, 4% *w*/*w*, and bis-ethylhexyloxyphenol methoxyphenyl triazine, 8% *w*/*w*) that can absorb the sun's UV rays and two bio-sunscreen ingredients (β-carotene, 0.1% *w*/*w*, and vitamin E, 0.1% *w*/*w*) that enable to scavenge free radicals and lessen UV radiation damage[41], were introduced to the oil phase, where olive oil was selected. The o/w emulsion gels were prepared as the encapsulation experiments (Fig. 4a) used water/oil mixing ratio with 4% *w*/*w* NP and 3% *w*/*w* PDMS-NH_2, and the morphology studies found that the loading of these anti-sunburn compounds did not change the structures of the emulsion gels (Supplementary Fig. 26). In addition, these emulsion gels are non-cytotoxic (Supplementary Fig. 27). Emulsion gel sample aside, an emulsion sample with the same components was prepared by vortex mixing. After these, another three groups, a blank sample, a UV sample (UV irradiation only), and a commercial sunscreen—L'Oreal sample were added to the in vivo experiments to evaluate their protection ability against UV-induced skin burn, where 20 mg sample dosage was swabbed evenly to the mouse dorsal with ~1 cm^2, and the swabbed skin area was subsequently irradiated by a high-intensity UV spot and the wound site was then recorded. Figure 4b showed the evolution of the irradiated area of one mouse in each group as a function of time. It was found that without any protection, the mouse was heavily burned with a huge wound (the UV group), and the wound got worse on 3rd day, partially healed with time, and left a ~0.12 cm^2 scar on 14th day. For the emulsion group, there was still a large area of the burned wound, showing insignificant protection on the skin due to the encapsulated active substances' quickly flowing away. The wound became much smaller if the mouse dorsal was coated with L'Oreal, as for example the wound area decreased from ~0.42 to ~0.11 cm^2 on 3rd day, showing a certain protection on the skin. Finally, the mouse was not injured by UV spot upon swab coating with the emulsion gels, as appearance (Fig. 4b), relative levels of melanin and erythema (Supplementary Fig. 28) were comparable to the blank group, which is consistent with the in vitro results, including their data variation in reactive oxygen species (ROS) generation (Supplementary Fig. 29) and mitochondrial membrane depolarization[42] (Supplementary Fig. 30). This indicates effective resistance to strong UV exposure by the absorption of encapsulated sunscreen ingredients in the emulsion gels (Supplementary Fig. 31) and the jammed interfacial monolayer NPs skeleton, providing efficient swab coating by excellent viscoelasticity.

Skin sections of the irradiated area for another batch of samples in the five groups on 3rd day were further histologically examined [using hematoxylin and eosin (H&E) staining]. Histological image of the blank mouse showed that the epidermis was intact and clear, the collagen fibers of the dermis were neatly arranged, and the subcutaneous tissue located below the dermis consisted of loose connective tissues, adipose tissues, and muscular layer (Fig. 5a). Upon UV irradiation, there was extensive loss of epidermis and large necrosis of the whole skin layer (black arrow), and one can see a large number of necrotic cell fragments with inflammatory cell infiltration (red arrows), showing a strongly irradiated dermatitis. Epidermal loss, necrosis of skin tissue and infiltration of inflammatory cells in the dermis and subcutaneous tissue were alleviated by coating emulsions, which can be attributed to the residual encapsulated active ingredients. For the L'Oreal group, there were only a small amount of epidermal cell degeneration (blue arrows) and epidermal thickening (Supplementary Fig. 32), and a small amount of inflammatory cell infiltration in the dermis and subcutaneous tissue. If the emulsion gels were coated on the skin, neither inflammation/damage to the epidermis, dermis, and subcutaneous tissue (Fig. 5a), nor keratin overproduction, was observed (Supplementary Figs. 33 and 34), akin to the histological morphology of the blank mouse.

After the local histological morphology examination, the quantitative pathology (the average data of the UV irradiated skin area),

https://doi.org/10.1038/s41467-024-55099-9

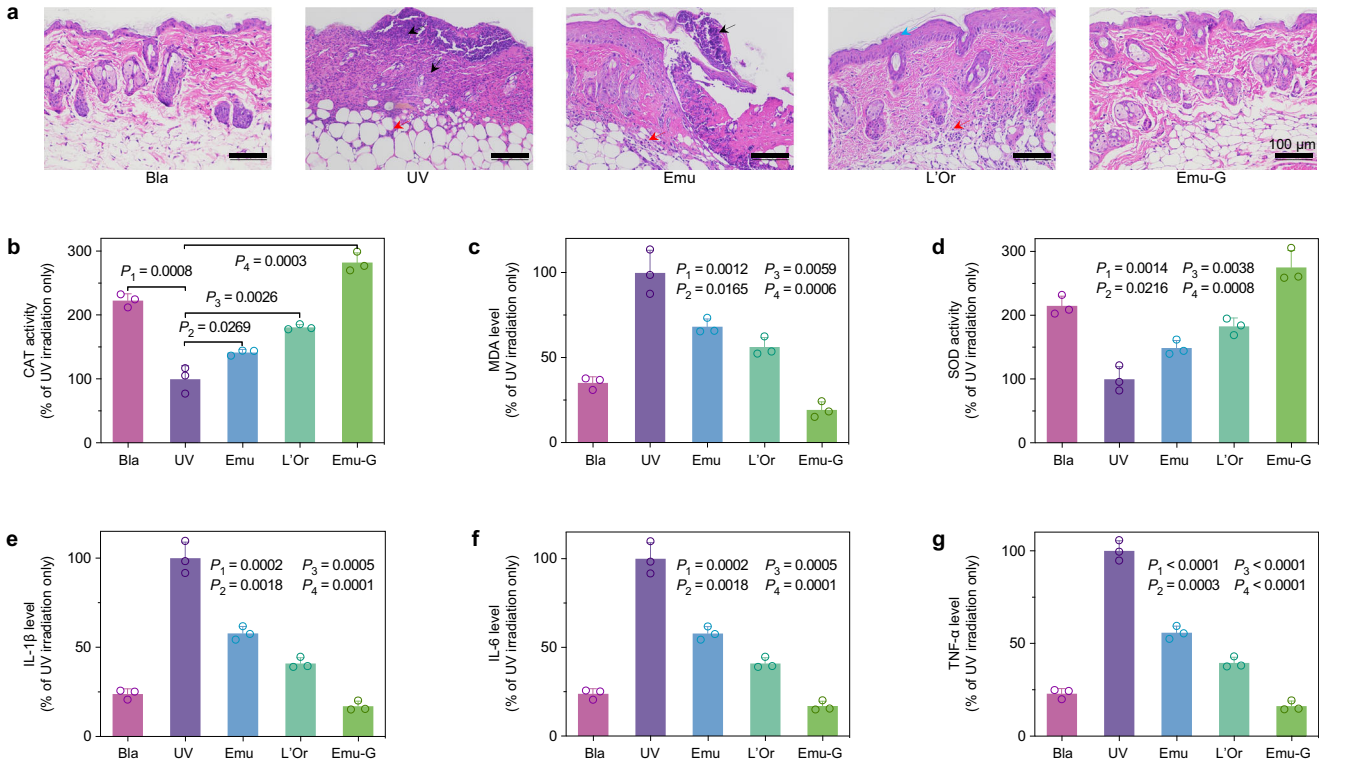

Fig. 5 | Histological examination and biochemical detection showing robust protection of emulsion gel against UV damage on mouse skin. a Histological images demonstrating the difference in injury of skin sections from the irradiated areas of five groups of mice collected on 3rd day. The black arrows point to the area of skin tissue necrosis. The red arrows point to the area of necrotic cell fragments with inflammatory cell infiltration. The blue arrows point to the area of epidermal cell degeneration. **b** The activity of CAT (an antioxidant enzyme), (**c**) the level of MDA (a final product of lipid peroxidation), and (**d**) the activity of SOD (another antioxidant enzyme) in homogenates of skin tissues from the irradiated areas of five groups of mice collected on 3rd day indicating their level of peroxidation of the skin. The levels of three inflammatory factors: (**e**) IL-1β, **f** IL-6, and (**g**) TNF-α in homogenates of skin tissues from the irradiated areas of five groups of mice collected on 3rd day indicating the extent of the inflammatory reaction of the skin. Data were collected based on the normalization of the UV group (UV irradiation only sample) as 100% and presented as mean ± SD of $n = 3$ biologically independent mice. *P*-values were derived from the two-sided Student's *t*-test to determine the difference between the two groups, and *P*-values < 0.05 were defined to be statistically significant. Bla represents the blank group, that mice were neither coated with samples nor irradiated with UV spot. UV represents the UV group, that mice were treated with UV irradiation. Emu, L'Or, and Emu-G represent the emulsion, L'Oreal and emulsion gel groups, that mice were swabbed with the same amount of emulsion, L'Oreal sunscreen, and emulsion gel sample before UV irradiation, respectively.

including oxidative stress and inflammation, was then probed. Here, we examined three oxidative stress-related factors (catalase: an antioxidant enzyme, CAT; malondialdehyde: a final product of lipid peroxidation, MDA; superoxide dismutase: another antioxidant enzyme, SOD[43,44]) and three inflammatory factors (interleukin-1 beta: IL-1β; interleukin-6: IL-6; and tumor necrosis factor-alpha: TNF-α[45,46]) of these groups' tissue homogenates. All data were collected based on the normalization of the UV group (UV irradiation only) as 100%. As shown in Fig. 5b–d, compared with the blank group, the skin tissues of mice irritated by the UV spot showed a decrease in CAT activity, from 223% to 100% ($P = 0.0008$, P is a number describing the statistically significant difference between the two sets of values; the smaller of P, the bigger of difference between them), and SOD activity, from 215% to 100% ($P = 0.0014$), and an increase in MDA level from 35% to 100% ($P = 0.0012$). It suggests that UV irradiation attenuated those two antioxidant enzymes, which resulted in the enhancement of peroxidation of local skin tissue and the damage of epidermal and dermis structures. With the coating of emulsions, L'Oreal or emulsion gels, the enhancement (in comparison with the UV group) of CAT and SOD activities gradually increased from 142% ($P = 0.0269$) to 181% ($P = 0.0026$) and to 282% ($P = 0.0003$), and from 149% ($P = 0.0216$) to 183% (0.0038) and to 275% ($P = 0.0008$) respectively; and the reduction in MDA level was observed from 68% ($P = 0.0165$) to 56% ($P = 0.0059$) and to 19% ($P = 0.0006$), indicating that the pretreatment of these three samples can improve the antioxidative activity of the skin, and reduce oxidative products and skin damage induced by UV irradiation, with the emulsion gel having the most significant effect. We note that the data of the emulsion gel group is better than that of the blank group. This arises from the swab coatability of our viscoelastic emulsion gels and their effective encapsulation of chemical substances to absorb the UV light, and the bioactive ingredients (β-carotene and vitamin E) may even increase the enzyme activity. Such robust protection of emulsion gels on the skin can also be seen in the results of those inflammatory factors (IL-1β, IL-6, and TNF-α), where they showed lower inflammatory factors than those of blank and L'Oreal groups (Fig. 5e–g), e.g. IL-1β level of 24%, 41% and 17% for the blank, L'Oreal, and emulsion gel groups. In addition, the inflammatory factors between other groups showed a similar trend with the results of oxidative stress indicators and H&E stained tissue sections. The above results show that our synthetic sunscreen can prevent UV-induced morphological and dermatopathologic abnormalities, thoroughly defeating the commercial L'Oreal product.

Discussion

In summary, bridged emulsion gels are achieved by employing a polymer to manipulate NP assembly at the water/oil interfaces, resulting in its three-phase contact angle at ~45°, bridging across droplets to form emulsion networks with shared facets. Eliminating the need for multiple steps of emulsification and gelation or extremely careful modifications of NPs and, the versatility of the chemicals of the

system, as the NP, the polymer, and the oil phase can all be varied, make the formulation greatly simple and general. Their microstructure and rheological properties can, if desired, be effectively manipulated by adjusting formulation conditions, including both components' concentrations and volume ratios. Selecting one of these emulsion gels with the large-amount encapsulation and storage ability as a proof of concept, a sunscreen cream was designed for skin care, exceeding in performance of the commercial L'Oreal products. More importantly, our synthetic sunscreen cream takes only seconds by mixing the water and the oil phases and, can be readily scalable, offering a viable approach for the next-generation cosmetic and ointment.

Methods

Materials

HS-40 Ludox (silicon dioxide, SiO_2, 40% *w*/*w* suspension in H_2O) with diameter of 12 nm and rhodamine B isothiocyanate dye (RITC) were purchased from Sigma-Aldrich. The pH of dilute dispersions of SiO_2 nanoparticles (NPs) was adjusted to 7.0 with HCl. Monoaminopropyl-terminated polydimethylsiloxanes (PDMS-NH_2, MW = 1000 g mol^{-1}) was purchased from Gelest. Monoamino-terminated polystyrenes (PS-NH_2, MW = 1500 g mol^{-1}) was purchased from Polymer Source. 3-aminopropyltriethoxysilane (APS, 97%) and Nile red (98%) were purchased from Meryer. Rhodamine B (98%) and tetraethyl orthosilicate (TEOS, 98%) were purchased from TCI. Ammonium hydroxide solution (25–28% *w*/*w*) and anhydrous ethanol (99.7%) were purchased from Titan. β-carotene (99.7%), *n*-hexane (99%), and tricaprylin (98%) were obtained from Aladdin. Olive oil, *n*-dodecane (99%), methylene bis-benzotriazolyl tetramethylbutyl phenol (98%), ethylhexyl triazone (98%), bis-ethylhexyloxyphenol methoxyphenyl triazine (98%), and vitamin E (99%) were purchased from Macklin. Toluene (99.9%) was purchased from Fisher. The human keratinocyte cell line (HaCaT) of male origin was purchased from Haixing Biosciences (TCH-C388) and identified via short tandem repeat (STR) profiling. The oxidation-sensitive fluorescent probe 2′,7′-Dichlorodihydrofluorescein diacetate (H2DCFDA), 5,5′,6,6′-tetrachloro-1,1′,3,3′-tetraethylbenzimidazolylcarbocyanine iodide (JC-1) and 2′-[4-ethoxyphenyl]-5-[4-methyl-1-piperazinyl]-2,5′-bi-1H-benzimidazole trihydrochloride trihydrate (Hoechst 33342) were purchased from Beyotime Biotechnology. Veet hair removal cream and L'Oreal sunscreen were purchased from Watson's. Catalase (CAT) and malondialdehyde (MDA) assay kits were purchased from Servicebio (#G4300-96T and #G4307). Superoxide dismutase (SOD) assay kit (#A001-1) was purchased from NanJing JianCheng Bioengineering Institute. ELISA assay kits to measure the levels of interleukin-1 beta (IL-1β), interleukin-6 (IL-6), and tumor necrosis factor-alpha (TNF-α) were purchased from BioLegend (#432615, #431315, and #430915). All reagents were used without further purification. Deionized (DI) water was used in all experiments.

Characterization

Fourier-transform infrared (FTIR) spectra of the commercial SiO_2 NPs was performed on a Nicolet iS50R spectrometer. The zeta potentials of aqueous dispersions of the commercial SiO_2 NPs and synthetic RITC-tagged SiO_2 NPs were performed on Malvern Zetasizer Nano ZS90 at 25 °C. Scanning electron microscopy (SEM) images of RITC-tagged SiO_2 NPs were obtained on an environmental scanning electron microscope (SU8010). The water/oil interfacial tension (γ) was probed by an interface viscoelastic measuring device (OCA 15EC) using the pendent-drop method, where the evolution of γ with time was recorded by injecting a pendent water drop into the toluene phase. Confocal microscopy images of bridged emulsion gels were recorded by an Olympus FV3000 confocal laser scanning microscope. Fluorescence microscopic images of emulsions were recorded by IX71. Cryo-electron microscopic images of bridged emulsion gels were obtained on an environmental scanning electron microscope (SU8010) with a cryogenic preparation transfer system. The rheological behaviors of bridged emulsion gels were obtained on a DHR-2 rheometer. Ultraviolet−visible (UV−vis) absorbance spectra of the bulk oil and the oil phases of bridged emulsion gels that were both loaded with β-carotene was performed on a UV-6100 spectrometer. The histological images of the mouse skin sections were collected by a Nikon Eclipse Ci-L plus upright microscope.

Preparation of RITC-tagged SiO_2 NPs

RITC-tagged SiO_2 NPs were synthesized according to the classical Stöber reaction[47,48]. First, the RITC-APS conjugate dye solution was prepared by adding RITC dye (12.5 mg) and APS (50 mg) to anhydrous ethanol (10 mL) and stirring for 12 h, and set aside. Then, anhydrous ethanol (35 mL), ammonium hydroxide solution (13.2 mL, 25 − 28% *w*/*w*), and RITC-APS conjugated dye solution (5 mL) were combined in a round-bottom flask. The NPs began to be grown by injecting a mixture of TEOS (5 mL) and anhydrous ethanol (5 mL) into the flask using a syringe mounted on a syringe pump (~50 μL min^{-1}) while stirring (300 rpm). After 12 h of reaction, the NPs were cleaned by centrifugation (1,1576 × *g*) in DI water 5 times and then dried at 70 °C in an oven for 4 h. The nanoparticles were dispersed in water for use. The scanning electron microscopy (SEM) images showed that the RITC-tagged SiO_2 NPs were nearly monodisperse with an average diameter of 630 nm.

Preparation of bridged emulsion gels and emulsions

Bridged emulsion gels were prepared by mixing the oil phase (toluene containing PDMS-NH_2 in different concentrations or containing PS-NH_2; or olive oil, *n*-hexane, tricaprylin or *n*-dodecane containing PDMS-NH_2) and the aqueous phase (DI water containing commercial SiO_2 NPs in different concentrations, or containing RITC-tagged SiO_2 NPs) in different volume ratios, and homogenizing (46 W for 14 s continuously) using an ultrasonic probe (SCIENTZ JY92-IIN). The stability of bridged emulsion gels against centrifugation was performed at different speeds (0 − 861 × g) for 1 min.

Emulsions (for in vivo experiment) were prepared by mixing the oil phase (olive oil containing PDMS-NH_2) and the aqueous phase (DI water containing commercial SiO_2 NPs) with a water/oil mixing ratio at 3:7, and stirring with Vortex QL-861 at 3000 rpm for 5 min.

Image analysis

The emulsion gels were imaged of dimension 1024 × 1024 pixels with a 60 × oil immersion objective using a laser scanning confocal microscopy. The three-dimensional (3D) stacks were created by taking up to 50 images in succession with a (nominal) increment in the z-direction. A series of slices were imported into the Avizo software (Visualization Sciences Group) to generate 3D ortho slice, and interactive thresholding was performed to obtain the thresholded images. Next, the surface module was generated, segmentation was performed, and the Gaussian curvature, *K*, could be calculated.

Cryo-scanning electron microscope (cryo-SEM) imaging

First, 0.5 μl of bridged emulsion gel was placed inside a hollow cylindrical sample stage and rapidly frozen in a liquid nitrogen jet freezer. After freezing, the sample was mounted onto a fracture cryo-stage under liquid nitrogen, transferred under inert gas in a cryo-high vacuum airlock to a pre-cooled freeze-fracture device, and fractured. Then, the samples were sublimated under vacuum at −50 °C for 15 min, followed by gold sputtering using a current of 10 mA for 2 min. Finally, the freeze-fractured, metal-coated samples were transferred in a pre-cooled (−140 °C) cryo-SEM (HITACHI SU8010) for imaging.

Rheological measurements of bridged emulsion gels

The viscoelastic properties of bridged emulsion gels were measured by a rotating rheometer equipped with two parallel flat plates of

diameter = 40 mm. The gap between the two plates was fixed at 0.5 mm. Each sample was first performed with a frequency sweep from 1 to 100 rad s^{-1} at a constant strain of 1 %, followed by a strain sweep from 0.1 to 1000% at a constant frequency of 10 rad s^{-1} at 25 °C. The temperature sweeps were conducted from 20 to 60 °C at a constant strain of 1 % and a constant frequency of 10 rad s^{-1}.

Storage stability of β-carotene in the bridged emulsion gels

Typically, an *n*-dodecane solution (560 μL) of β-carotene (0.1% *w*/*w*) and PDMS-NH_2 (3% *w*/*w*) was homogenized with aqueous dispersions (240 μL, 1, 2, 4% *w*/*w*, respectively) of SiO_2 NPs to give o/w bridged emulsion gels. All samples were flushed with a nitrogen stream for 15 min, then sealed and placed in a 37 °C water bath for 35 days. At different time intervals, 0.5 g of the emulsion gel was taken and added to 2 mL of ethanol, followed by vortex mixing (3,000 rpm for 5 min) to destroy the gel structure. Then 3 mL of *n*-hexane was added to extract the β-carotene and repeated twice. The content of β-carotene was determined by the absorbance-concentration of the β-carotene standard curve at 453 nm using a UV–vis spectrophotometer. The retention of β-carotene in the bridged emulsion gels can be calculated as: C_t/C_0, where C_t and C_0 are the content of β-carotene at *t* and 0 days. A bulk *n*-dodecane (12 mL) of β-carotene (0.1% *w*/*w*) was treated in the same manner as a control.

The encapsulation rate and loading capacity of bridged emulsion gels was calculated as follows:

$$\text{Encapsulation rate}(\%) = \frac{Total\ mass\ of\ entrapped\ \beta-\text{carotene}}{Total\ mass\ of\ input\ \beta-\text{carotene}} \times 100 \quad (1)$$

$$\text{Loading capacity}(\mu g/mg) = \frac{Total\ mass\ of\ entrapped\ \beta-\text{carotene}}{Total\ mass\ of\ nanoparticle\ in\ emulsion\ gel} \quad (2)$$

The UV stability was estimated by exposing the samples to UV light (365 nm) for 6 h, and thermal stability was evaluated by subjecting samples to temperature conditions of 30 °C, 40 °C, 50 °C, 60 °C, and 70 °C within a water bath for a duration of 30 min.

UV shielding rate measurement

The emulsion gels for skin protection, mimicking the sunscreen cream, were prepared by homogenizing the olive oil (560 μL, containing 3% *w*/*w* PDMS-NH_2, 8% *w*/*w* methylene bis-benzotriazolyl tetramethylbutyl phenol, 4% *w*/*w* ethylhexyl triazone, 8% *w*/*w* bis-ethylhexyloxyphenol methoxyphenyl triazine, 0.1% *w*/*w* β-carotene and 0.1% *w*/*w* vitamin E) and the aqueous dispersion (240 μL, 4% *w*/*w*) of SiO_2 NPs. The emulsion prepared by vortex mixing with the same components as emulsion gel, and L'Oreal product [sun protection factor (SPF) 50 + , PA ++++] were as controls.

Emulsion, L'Oreal sunscreen and emulsion gel were painted on quartz slides with a thickness of 15 μm. The painted quartz slides were irradiated with a high-intensity UV spot (HOWSUPER, DGY-2, 365 nm) after 30 min. Then using a 365 nm light power meter to calculate the corresponding UV shielding rate.

In vitro cytotoxicity

The cytotoxicity of emulsion gels on HaCaT cells was assessed using Cell Counting Kit-8 (CCK-8) assay. Briefly, HaCaT cells were cultured in a complete medium solution at 37 °C with 5% CO_2. The cells were then seeded in 96-well plates at a density of 1×10^4 cells/well and incubated in 100 μL of complete medium solution at 37 °C in a humidified atmosphere of 5% CO_2 for 12 h to allow them to attach to the bottom of the plate. Subsequently, the cells were treated with emulsion gels at different concentrations (0.5, 1, 2, 5, and 10 mg mL^{-1}). Cells treated with PBS were used as control. After 24 h of incubation, CCK-8 kit was added and cell viability was calculated by measuring the absorbance of each well at 450 nm with a microplate reader (Multiskan MK3, Thermo Fisher Scientific, USA).

In vitro protection by emulsion gels against UV-induced ROS generation

50 mg of emulsion gel was applied to a thin quartz sheet fixed at 1 cm above the HaCaT cell culture dishes. The cells (~2×10^5 cells/dish) were then irradiated with a high-intensity UV spot (HOWSUPER, DGY-2, 365 nm, 270 mJ cm^{-2}). The emulsion and L'Oreal product were similarly tested. Cells without treatment served as the blank. Cells treated with UV irradiation served as the control. The production of ROS was monitored using an oxidation-sensitive fluorescent probe (H2DCFDA) and visualized by a confocal microscopy.

Mitochondrial membrane depolarization measurement

50 mg of emulsion gel was applied to a thin quartz sheet fixed at 1 cm above the HaCaT cell culture dishes. The cells (~2×10^5 cells/dish) were then irradiated with a high-intensity UV spot (HOWSUPER, DGY-2, 365 nm, 270 mJ cm^{-2}). The emulsion and L'Oreal product were similarly tested. Cells without treatment served as the blank. Cells treated with UV irradiation served as the control. The mitochondrial membrane potential was monitored by the fluorescent dye JC-1. Hoechst 33342 suggests the nuclei. The mitochondrial membrane depolarization was observed by confocal microscopy.

In vivo protection by emulsion gels from UV-induced skin burn

The hairs on the back of the BALB/c mice (8 weeks old, 18–20 g, female) were removed using an electric shaver, and then the shaved area was treated with hair removal cream. After 5 min, hair removal cream was wiped away and the dorsal skin was washed with water. The depilated mice were used for subsequent experiments after 24 h. All mice were housed in individually ventilated cages and maintained on a 12 h light/dark cycle at room temperature (25± 1 °C) with constant humidity (55 ± 10%). All mice were supplied with food and water ad libitum.

Mice were anesthesia with 1.5% isoflurane by inhalation. Skin burn was induced using a high-intensity UV spot (HOWSUPER, DGY-2, 365 nm). The UV spot was fixed above the anesthetized mice (height: 2.5 cm, 325 mW cm^{-2}) and irradiated for 6 min. The mice were photographed for 14 days to record the change of the irradiated site. The melanin and erythema values of the mouse skin were also measured after irradiation.

To evaluate the protection ability of the emulsion gels against UV-induced skin burn, 20 mg cm^{-2} emulsion gel samples were swabbed evenly to the mouse dorsal (~1 cm^2) of the depilated BALB/c mice (five/group) before UV irradiation. The emulsion and L'Oreal product were similarly tested. Mice without treatment served as the blank. Mice treated with UV irradiation served as the control.

Histological examination

The skin tissues from sacrificed mice were taken and fixed in a 4% paraformaldehyde solution. The fixed tissues were then embedded in paraffin, sectioned, and stained with H&E and Masson's trichome for observation. The epidermal thickness of the injured area and the keratin percentage were measured using ImageJ based on H&E staining images and trichome staining images, respectively.

Biochemical analysis

The skin tissues from sacrificed mice were taken, cut into pieces, and washed with pre-cooled phosphate buffer saline (PBS) to remove residual blood. PBS was mixed with the tissues at a weight ratio of 10:1. The tissues were then lysed using a tissue grinder, the homogenates were centrifuged at 13,776 × g for 5 min, and the supernatants were collected for biochemical detection. A CAT assay kit was used to

measure the activity of CAT. A MDA assay kit was used to measure the level of MDA. A SOD assay kit was used to measure the activity of SOD. ELISA assay kits were used to measure the levels of IL-1β, IL-6, and TNF-α. The procedures were performed according to the manufacturer's instructions.

Animals

All animal procedures were performed in accordance with Huazhong University of Science and Technology animal use rules and the requisite approvals of animal use committees (Approval No. [2023] IACUC Number: 4135). Eight-week-old BALB/c female mice were purchased from the Hubei Provincial Center for Disease Control and Prevention.

Statistics and reproducibility

GraphPad Prism 10 software (San Diego, USA) was used to create visual graphs and to calculate the statistical significance. Data were expressed as mean ± SD ($n = 3$). *P*-values were derived from the two-sided Student's *t*-test to determine the difference between the two groups, and *P*-values < 0.05 were defined to be statistically significant. Each experiment was repeated three times independently with similar results, e.g. images in Figs. 1c, d and 2a, b, d are representative of three repetitions.

Reporting summary

Further information on research design is available in the Nature Portfolio Reporting Summary linked to this article.

Data availability

All data supporting the findings of this study are available within the article and its supplementary files. All data underlying this study are available from the corresponding author upon request. Source data are provided with this paper.

References

1. Alexander, A. E. Practical emulsions. *Nature* **152**, 371 (1943).
2. Villar, G., Graham, A. D. & Bayley, H. A tissue-like printed material. *Science* **340**, 48–52 (2013).
3. Li, S. et al. Perfluorodecalin-based oxygenated emulsion as a topical treatment for chemical burn to the eye. *Nat. Commun.* **13**, 7371 (2022).
4. Xia, Y. et al. Exploiting the pliability and lateral mobility of Pickering emulsion for enhanced vaccination. *Nat. Mater.* **17**, 187–194 (2018).
5. Wei, Y., Cheng, G., Ho, H.-P., Ho, Y.-P. & Yong, K.-T. Thermodynamic perspectives on liquid–liquid droplet reactors for biochemical applications. *Chem. Soc. Rev.* **49**, 6555–6567 (2020).
6. Feng, Y. et al. A ferroptosis-targeting ceria anchored halloysite as orally drug delivery system for radiation colitis therapy. *Nat. Commun.* **14**, 5083 (2023).
7. Han, X. et al. Zwitterionic micelles efficiently deliver oral insulin without opening tight junctions. *Nat. Nanotechnol.* **15**, 605–614 (2020).
8. Amstad, E. Capsules made from prefabricated thin films. *Science* **359**, 743 (2018).
9. Sheng, J. et al. Synergetic treatment of oxygen microcapsules and lenvatinib for enhanced therapy of HCC by alleviating hypoxia condition and activating anti-tumor immunity. *Chin. Chem. Lett.* **34**, 107738 (2023).
10. Lu, X., Katz, J. S., Schmitt, A. K. & Moore, J. S. A robust oil-in-oil emulsion for the nonaqueous encapsulation of hydrophilic payloads. *J. Am. Chem. Soc.* **140**, 3619–3625 (2018).
11. Brown, C. et al. Assessment of single screening questions for dysphagia for routine clinical use in a tertiary care practice. *J. Clin. Oncol.* **32**, 102 (2014).
12. Downs, F. G. et al. Multi-responsive hydrogel structures from patterned droplet networks. *Nat. Chem.* **12**, 363–371 (2020).
13. Zarzar, L. D. et al. Dynamically reconfigurable complex emulsions via tunable interfacial tensions. *Nature* **518**, 520–524 (2015).
14. Dai, X. et al. Induction of tumor ferroptosis-dependent immunity via an injectable attractive Pickering emulsion gel. *Adv. Mater.* **35**, 2303542 (2023).
15. Rey, M. et al. Interactions between interfaces dictate stimuli-responsive emulsion behaviour. *Nat. Commun.* **14**, 6723 (2023).
16. Yan, T. et al. Widely adaptable oil-in-water gel emulsions stabilized by an amphiphilic hydrogelator derived from dehydroabietic acid. *Angew. Chem. Int. Ed.* **59**, 637–641 (2020).
17. Niu, X. et al. Structured emulgels by interfacial assembly of terpenes and nanochitin. *ACS Nano* **17**, 25542–25551 (2023).
18. Torres, O., Tena, N. M., Murray, B. & Sarkar, A. Novel starch based emulsion gels and emulsion microgel particles: design, structure and rheology. *Carbohydr. Polym.* **178**, 86–94 (2017).
19. Collison, R. & McDonald, M. P. Broadening of the water proton line in high-resolution nuclear magnetic resonance spectra of starch gels. *Nature* **186**, 548–549 (1960).
20. Tsurusawa, H., Arai, S. & Tanaka, H. A unique route of colloidal phase separation yields stress-free gels. *Sci. Adv.* **6**, eabb8107 (2020).
21. Lee, M. N., Chan, H. K. & Mohraz, A. Characteristics of Pickering emulsion gels formed by droplet bridging. *Langmuir* **28**, 3085–3091 (2012).
22. Wang, X.-Y. & Heuzey, M.-C. Pickering emulsion gels based on insoluble chitosan/gelatin electrostatic complexes. *RSC Adv.* **6**, 89776–89784 (2016).
23. Wu, B. et al. Attractive Pickering emulsion gels. *Adv. Mater.* **33**, 2102362 (2021).
24. Li, Z., Ming, T., Wang, J. & Ngai, T. High internal phase emulsions stabilized solely by microgel particles. *Angew. Chem. Int. Ed.* **48**, 8490–8493 (2009).
25. Jiao, B., Shi, A., Wang, Q. & Binks, B. P. High-internal-phase Pickering emulsions stabilized solely by peanut-protein-isolate microgel particles with multiple potential applications. *Angew. Chem. Int. Ed.* **57**, 9274–9278 (2018).
26. Yuan, L., Chen, L., Chen, X., Liu, R. & Ge, G. In situ measurement of surface functional groups on silica nanoparticles using solvent relaxation nuclear magnetic sesonance. *Langmuir* **33**, 8724–8729 (2017).
27. Chai, Y. et al. Direct observation of nanoparticle-surfactant assembly and jamming at the water-oil interface. *Sci. Adv.* **6**, eabb8675 (2020).
28. Huang, C. et al. Structured liquids with pH-triggered reconfigurability. *Adv. Mater.* **28**, 6612–6618 (2016).
29. Cui, M., Emrick, T. & Russell, T. P. Stabilizing liquid drops in nonequilibrium shapes by the interfacial jamming of nanoparticles. *Science* **342**, 460–463 (2013).
30. Liu, X. et al. Reconfigurable ferromagnetic liquid droplets. *Science* **365**, 264–267 (2019).
31. Huang, C. et al. Bicontinuous structured liquids with sub-micrometre domains using nanoparticle surfactants. *Nat. Nanotechnol.* **12**, 1060–1063 (2017).
32. Zanini, M. et al. Universal emulsion stabilization from the arrested adsorption of rough particles at liquid-liquid interfaces. *Nat. Commun.* **8**, 15701 (2017).
33. Wan, C. et al. Reversible emulsions from polyoxometalate–polymer: a robust strategy to cyclic emulsion catalysis and high-internal-phase emulsion materials. *J. Am. Chem. Soc.* **145**, 25431–25439 (2023).
34. Vaessen, G. E. J., Visschers, M. & Stein, H. N. Predicting catastrophic phase inversion on the basis of droplet coalescence kinetics. *Langmuir* **12**, 875–882 (1996).

35. Wang, Q. et al. High-water-content mouldable hydrogels by mixing clay and a dendritic molecular binder. *Nature* **463**, 339–343 (2010).
36. Zhang, Y. S. & Khademhosseini, A. Advances in engineering hydrogels. *Science* **356**, eaaf3627 (2017).
37. Sun, G., Li, Z. & Ngai, T. Inversion of particle-stabilized emulsions to form high-internal-phase emulsions. *Angew. Chem. Int. Ed.* **49**, 2163–2166 (2010).
38. Triantafillidis, C., Elsaesser, M. S. & Hüsing, N. Chemical phase separation strategies towards silica monoliths with hierarchical porosity. *Chem. Soc. Rev.* **42**, 3833–3846 (2013).
39. Ikem, V. O., Menner, A. & Bismarck, A. High internal phase emulsions stabilized solely by functionalized silica particles. *Angew. Chem. Int. Ed.* **47**, 8277–8279 (2008).
40. Zbyradowski, M. et al. Triplet-driven chemical reactivity of β-carotene and its biological implications. *Nat. Commun.* **13**, 2474 (2022).
41. Nachtsheim, B. J. Creating antioxidants by oxidation catalysis. *Science* **345**, 270–271 (2014).
42. Wang, C. et al. Skin pigmentation-inspired polydopamine sunscreens. *Adv. Funct. Mater.* **28**, 1802127 (2018).
43. Melov, S. et al. Extension of life-span with superoxide dismutase/catalase mimetics. *Science* **289**, 1567–1569 (2000).
44. Weismann, D. et al. Complement factor H binds malondialdehyde epitopes and protects from oxidative stress. *Nature* **478**, 76–81 (2011).
45. Sliter, D. A. et al. Parkin and PINK1 mitigate STING-induced inflammation. *Nature* **561**, 258–262 (2018).
46. Cao, F. et al. Artificial-enzymes-armed bifidobacterium longum probiotics for alleviating intestinal inflammation and microbiota dysbiosis. *Nat. Nanotechnol.* **18**, 617–627 (2023).
47. Bogush, G. H., Tracy, M. A. & Zukoski, C. F. Preparation of monodisperse silica particles: control of size and mass fraction. *J. Non-Cryst. Solids* **104**, 95–106 (1988).
48. Blaaderen, A. & Vrij, A. Synthesis and characterization of colloidal dispersions of fluorescent, monodisperse silica spheres. *Langmuir* **8**, 2921–2931 (1992).

Acknowledgements

This work was supported by the National Natural Science Foundation of China [No. 52293474 (J.Z.), 22275063 (C.H.) and 21903033 (C.H.)], and the start-up funds from Huazhong University of Science and Technology. We would also like to acknowledge the Scientific research sharing platform of the College of Life Science and Technology at Huazhong University of Science and Technology (HUST) for confocal microscopy imaging and analysis.

Author contributions

C.H. designed and directed the experiments. C.W. performed most of the experiments, analyzed the data and wrote the paper. Q.C., Y.S. and X.Y. contributed to the data analyses. K.D. and H.J. performed the in vitro experiments. S.H. and C.M. assisted the in vivo experiments. C.H., J.X. and J.Z. contributed to the manuscript revision. All authors read and approved the final version of the manuscript.

Competing interests

The authors declare no competing interests.

Additional information

Supplementary information The online version contains supplementary material available at https://doi.org/10.1038/s41467-024-55099-9.

Correspondence and requests for materials should be addressed to Caili Huang.

Peer review information *Nature Communications* thanks Qiang Xia, and the other, anonymous, reviewer(s) for their contribution to the peer review of this work. A peer review file is available.